

Aridity is expressed in river topography globally

Shiuan-An Chen^{1*}, Katerina Michaelides^{1,2*}, Stuart W. D. Grieve³ & Michael Bliss Singer^{2,4,5}

It has long been suggested that climate shapes land surface topography through interactions between rainfall, runoff and erosion in drainage basins^{1–4}. The longitudinal profile of a river (elevation versus distance downstream) is a key morphological attribute that reflects the history of drainage basin evolution, so its form should be diagnostic of the regional expression of climate and its interaction with the land surface^{5–9}. However, both detecting climatic signatures in longitudinal profiles and deciphering the climatic mechanisms of their development have been challenging, owing to the lack of relevant global data and to the variable effects of tectonics, lithology, land surface properties and human activities^{10,11}. Here we present a global dataset of 333,502 river longitudinal profiles, and use it to explore differences in overall profile shape (concavity) across climate zones. We show that river profiles are systematically straighter with increasing aridity. Through simple numerical modelling, we demonstrate that these global patterns in longitudinal profile shape can be explained by hydrological controls that reflect rainfall–runoff regimes in different climate zones. The most important of these is the downstream rate of change in streamflow, independent of the area of the drainage basin. Our results illustrate that river topography expresses a signature of aridity, suggesting that climate is a first-order control on the evolution of the drainage basin.

Conventional theory presents river longitudinal profiles (long profiles) as having a generally concave-up shape, with knickpoints and other fluctuations expressing the interactions of several independent variables: climate, tectonics, lithology and human impacts^{11–13}. This characteristic shape of long profiles has been interpreted to arise as a result of downstream flow increase with drainage area, which erodes the riverbed, transports sediment from upstream to downstream, and produces fining profiles in the grain size of riverbed material^{13,14}. However, there are long profiles with overall concavity much closer to zero (that is, the profiles are straighter than the typical concave-up profile shape)^{15–17}, yet there is limited understanding of the global distribution of long profile concavities and their relation to climate. Stream power incision theory states that channel erosion is intrinsically tied to an assumed relationship between river discharge (Q) and drainage area (A): $Q \propto A^c$. On the basis of this theory, an expression has been derived¹⁸ that links supply-limited river long profile concavity to the exponent c , illustrating that profiles will be concave up for $c > 0$, straight for $c = 0$, and convex for $c < 0$. A similar dependency of profile concavity on the Q - A relationship has been derived for transport-limited fluvial systems¹⁹. Previous work has largely emphasized long profile concavity for cases where $c > 0$, despite evidence that c in many river basins, especially in drylands, may vary from flood to flood over a range from negative to positive values^{8,17,20}. Of particular interest here is to ascertain whether the climatic expression within river channel hydrology may be a first-order control on long profile shape, and whether its climatic signature is preserved across the globe.

A river experiences a cascade of influences from climate to hydrology to erosion, which evolves its long profile. Therefore, the climatic expression within streamflow should be a first-order control on long profile shape^{6–8}. Numerical analysis of profile shape responses to a

distribution of flow events above the threshold for bedrock incision has demonstrated part of this dependency^{5,8,21}. However, there is limited global evidence of how the hydrologic expression of climate affects long profiles, across a wide range of climate zones. Climate determines the precipitation regime within a region. In turn, the precipitation regime controls the rate and frequency of water supply to the land surface, a proportion of which generates runoff over drainage basins, subject to losses by infiltration and evapotranspiration. Flow in rivers occurs when runoff reaches the channel, with notable baseflow contributions in humid regions from groundwater and subsurface drainage and potential for prolonged periods of no flow in arid channels. The flow of water within a river is a key driver of landscape evolution, through the corresponding downstream force exerted on the stream bed, the associated channel erosion, and the expression of local river incision at each elevation position along the long profile. Therefore, we propose that the climate–streamflow relationship exerts a strong control on long profiles.

Climate is expressed differently in the downstream rate of change in streamflow between arid and humid endmember rivers. In arid climates, streamflow tends to decrease downstream in all but extreme floods²² for two main reasons. First, low annual rainfall, limited areal coverage of rainstorms, and short duration of rainfall events generates partial area runoff²³. This results in a small proportion of basin tributaries contributing streamflow to the mainstem for limited periods of time. Second, rivers are typically ephemeral (having no permanent flow)²⁴, so channels lose water through dry, porous beds (transmission losses²²) because water tables lie well below the channel²⁵. Thus, the often-assumed power-law relationship between streamflow and drainage area (with positive exponent c) breaks down²⁰, such that the long-term average value of c may be negative, positive or zero. By contrast, humid channels have perennial flow (all year round), supported by baseflow from groundwater, and they accumulate flow from adjoining tributaries, producing downstream increases in discharge¹³ (positive c). We intuit that there is a spectrum of prevailing downstream changes in streamflow across the globe based on the regional expression of climate within discharge regimes (for example, dryland hydrology or mountain front orography⁵), rather than simply on drainage basin area. Given the obvious link between streamflow and riverbed erosion, we hypothesize that climatic signatures are imprinted within river long profiles, superimposed upon other exogenous controls. In other words, we expect a great deal of scatter, as is typical of environmental data, but we hypothesize that climate will reveal itself as a first-order control on long profile shape.

To test this hypothesis, we produced a database of global longitudinal profiles (GLoPro) of rivers between 60° N and 56° S (Fig. 1) extracted from NASA's 30-m-resolution Shuttle Radar Topography Mission Digital Elevation Model (SRTM-DEM)²⁶. The profiles were extracted using LSDTopoTools²⁷, software with advanced capabilities in topographic analysis, employing a conservative threshold for upstream drainage area and an algorithm for channel extraction, both of which reduce the likelihood of including non-channel features (see Methods). For each profile we computed the Normalized Concavity Index (NCI), a metric computed solely on the basis of profile geometry (Methods;

¹School of Geographical Sciences, University of Bristol, Bristol, UK. ²Earth Research Institute, University of California Santa Barbara, Santa Barbara, CA, USA. ³School of Geography, Queen Mary University of London, London, UK. ⁴School of Earth and Ocean Sciences, Cardiff University, Cardiff, UK. ⁵Water Research Institute, Cardiff University, Cardiff, UK. *e-mail: sc16970@bristol.ac.uk; katerina.michaelides@bristol.ac.uk

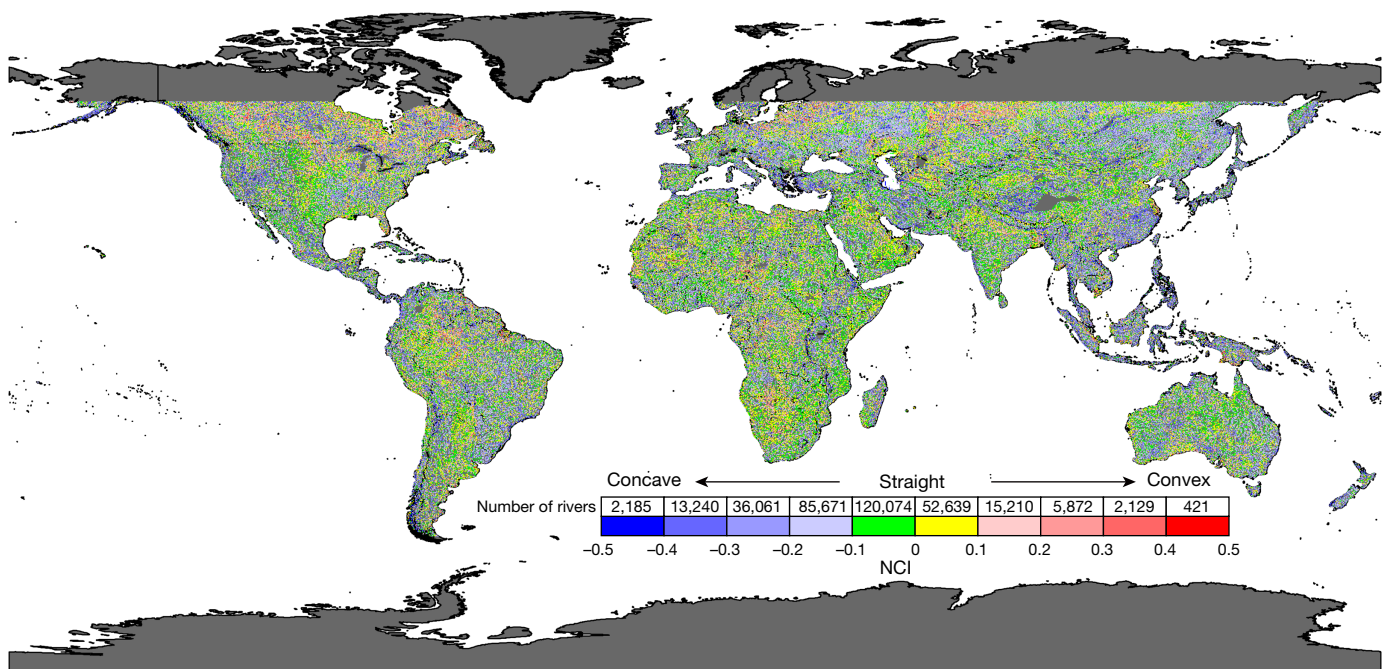


Fig. 1 | Global map of extracted river long profiles classified by NCI values. Each dot identifies the most downstream point of each extracted river profile, colour-coded by NCI value. River long profiles were extracted from the 30-m-resolution SRTM-DEM, which covers land area between

60° N and 56° S. The inset table shows the number of extracted rivers in each NCI bin. The free vector and raster background map is from Natural Earth (<https://www.naturalearthdata.com/>) in the Pseudo Plate Carrée map projection in ArcGIS.

Extended Data Fig. 1) that allows for standardized comparisons of river profile shapes across the globe. The NCI is negative if the profile is concave-up, zero if the profile is straight, and positive if the profile is convex-up.

We categorized each profile in GLoPro using the Köppen–Geiger climate classification²⁸ and the quantitative Aridity Index (calculated by dividing precipitation by potential evapotranspiration)²⁹, to investigate relationships between climate and the shape of the river long profile and to test whether the expression of aridity is detectable in NCI. The Köppen–Geiger classification is based on temperature and precipitation thresholds, emphasizing the response of vegetation to climate. The Aridity Index is a scale that represents the balance between precipitation and evaporative demand, and it declines with aridity. Here we addressed the null hypothesis that there are no differences in NCI between climate categories. We did not censor GLoPro for any other natural or anthropogenic factors, and it includes both bedrock and alluvial rivers. We do not make any assumptions about whether the profiles are steady-state (equilibrium) or transient, but we assumed that climate categories in the Köppen–Geiger classification and the Aridity Index have not changed substantially over the timescales of long profile development (Methods).

The global distribution of NCI values does not suggest any strong geographic biases, although there are clear concentrations of convex (southern Siberia), concave (southeast Asia), and nearly straight (Arabian peninsula) rivers (Fig. 1). NCI distributions of different climate classes (Fig. 2a) overlap and display great breadth, reflecting the large sample size and the many interacting independent variables (climate, tectonics, lithology and human factors) that affect drainage basin development. Nevertheless, statistically significant differences between distributions are evident (P values are between 1×10^{-250} and 1.48×10^{-22} , Extended Data Fig. 5). Comparing the four main Köppen–Geiger climate zones, all NCI distributions are negatively skewed, revealing that river long profiles are generally concave-up (Fig. 2a). However, compared to the other three main climate zones (Tropical, Temperate and Cold), the NCI values for Arid zone rivers are notably closer to zero (straighter) with a narrower distribution (Extended Data Table 1). The distinct signature of straighter

profiles within the Köppen–Geiger Arid climate zone in GLoPro is an unprecedented finding. To further explore this result, we investigated the relationship between NCI for the Aridity Index climate classification, ranging from Humid to Hyper-Arid categories. We found a systematic increase in NCI distribution medians from concave-up to straighter profiles as aridity increases (Fig. 2c, d). Furthermore, we found (Fig. 2e) a higher frequency of concave river profiles within humid regions (combining the Dry Sub-Humid and Humid categories of the Aridity Index), and a higher frequency of straighter profiles in drylands (combining the Hyper-Arid, Arid and Semi-Arid categories of the Aridity Index). In other words, the straightness of the long profile appears to be directly related to the water balance of a region, and by extension so is its expression within streamflow regimes that erode riverbeds.

We asked why arid river long profiles are straighter than humid ones and how climate influences the long profile through its expression in streamflow. Stream power theory indicates that the variation of discharge with drainage area influences long profile concavity for supply-limited channels. We sought to relax this assumption of Q–A dependency and thus provide a more general mechanistic explanation of our GLoPro results, and one that applies to transport-limited channels. We used the numerical model LONGPRO³⁰ (Methods), and distilled the hydrological expression of climate within a parameter representing the downstream rate of change in streamflow, which replaces the Q–A relationship from stream power theory. Specifically, discharge changes with distance down the channel at a rate controlled by the power law exponent, α , in the equation: $Q_L = Q_n(L/L_n)^\alpha$, where Q_L is the discharge at a distance downstream, L , and n is the most downstream point on the profile (Methods). We simulated the evolution of river long profiles using six values of α that together represent a range of downstream decreasing and increasing discharge rates ($\alpha = -2, -1, -0.5, 0.5, 1, 2$). We kept all other LONGPRO model parameters constant within established ranges for natural rivers but we explored their influence on NCI separately (Methods). For each simulated profile, we calculated the NCI value (Fig. 3a).

We found that NCI in the simulated profiles is systematically influenced by α (Fig. 3b). Specifically, the fastest downstream decreasing

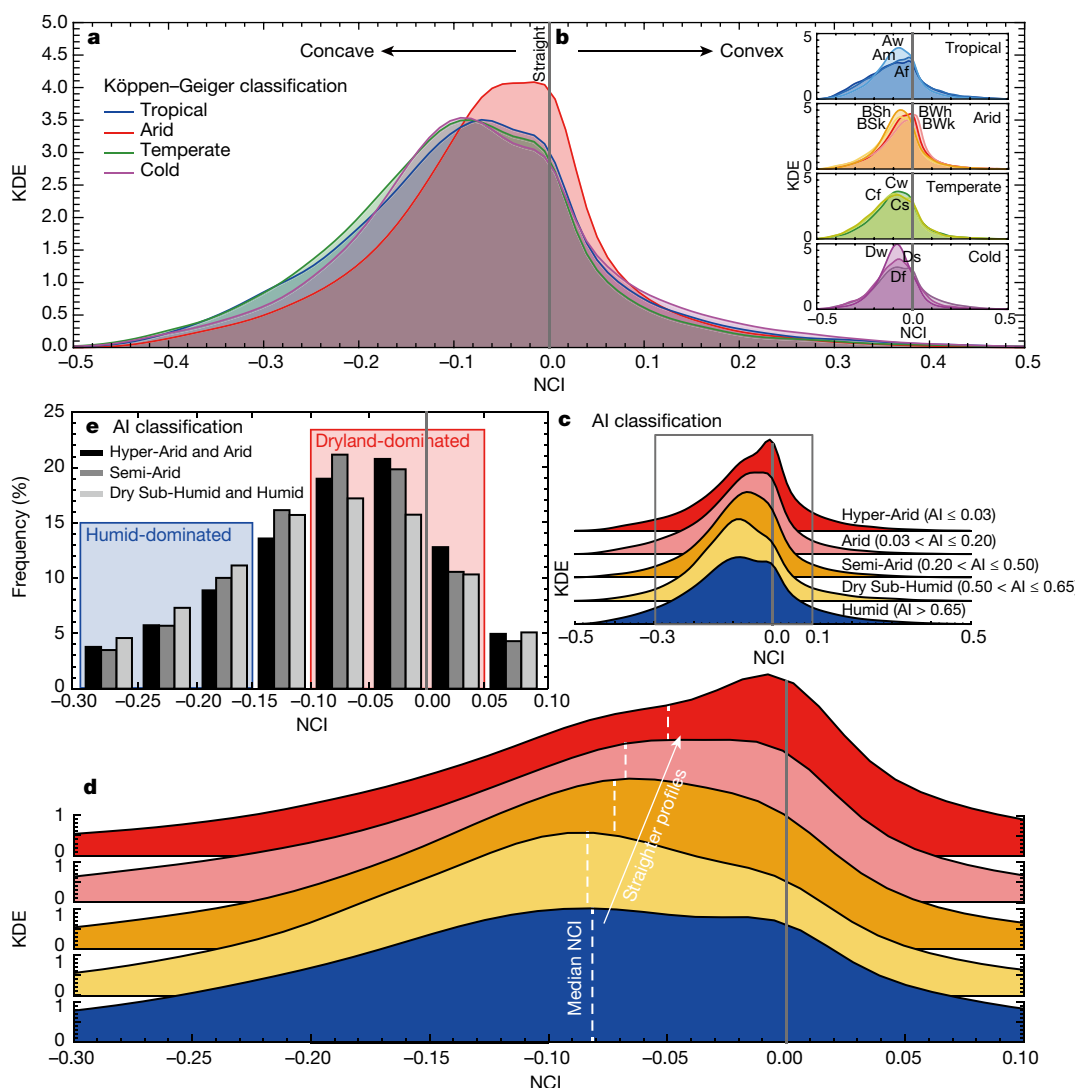


Fig. 2 | Effect of climate on NCI. Kernel density estimation (KDE) (see Methods) is a nonparametric representation of the probability density function. **a, b,** Comparisons of NCI values for four main Köppen–Geiger climate zones, highlighting the distinctiveness of Arid zone concavities (a) and the sub-zones of the Köppen–Geiger classification, including Tropical–rainforest (Af), Tropical–monsoon (Am), Tropical–savannah (Aw), Arid–hot desert (BWh), Arid–cold desert (BWk), Arid–hot steppe (BSh), Arid–cold steppe (BSk), Temperate–dry summer (Cs), Temperate–dry winter (Cw), Temperate–without dry season (Cf), Cold–dry summer

(Ds), Cold–dry winter (Dw) and Cold–without dry season (Df). **(b, c, d,** KDE values versus NCI values for Aridity Index (AI) climate categories (**d** is an enlargement of the rectangle in **c**, showing variations in NCI distributions based on the Aridity Index). **e,** Frequencies of combined Aridity Index categories between NCI distributions, highlighting dryland-dominated and humid-dominated bins of NCI values, where dryland includes the Hyper-Arid, Arid and Semi-Arid categories and humid includes the Dry Sub-Humid and Humid categories. The grey vertical line on each plot represents straight profiles (NCI = 0).

discharge ($\alpha = -2$) produces convex-up profiles and profiles become progressively straighter and then concave-up with increasing α . In general, long profiles are straighter when α approaches zero (discharge does not vary downstream). These LONGPRO results provide definitive mechanistic support to our NCI results from GLoPro, and they also corroborate the effect of the exponent c on concavity from stream power theory, pointing to aridity and its influence on downstream discharge as a first-order control on longitudinal profile shape.

We tested the representativeness of the modelled α values for real rivers by analysing flow data from a range of gauged rivers in the USA (Methods). The analysis reveals ranges of α consistent with expectations for each Köppen–Geiger climate zone, whereby Tropical, Temperate and Cold zones exhibit large, positive α values, and the Arid zone displays α values close to zero (Extended Data Fig. 8a). Note that a range of α values (positive, negative and zero) is probably common to arid rivers owing to the variable expression of climate within stream hydrology on a flood-by-flood basis^{17,20}. Furthermore, the median value of α is affected by long periods of no

flow (ephemerality), typical of dryland rivers (Extended Data Fig. 8b). Ephemeral accentuates transmission losses that reduce downstream flow and also gives more weight to each historical flood event; that is, smaller floods that exhibit downstream decreasing discharge are more frequent yet less geomorphically effective than large ones that increase downstream^{4,17}. Thus, α may vary between negative and positive values for each flood, resulting in a distributional median value close to zero.

Combining these hydrologic data with our model results enables interpretation of the global trends in long profile concavities with aridity, revealing three results. (1) The concave-up river profile can develop solely as a result of perennial flow conditions and downstream flow increase, consistent with stream power incision theory¹⁸. (2) Straighter long profiles can evolve in rivers that flow infrequently and for which the median discharge is similar everywhere along the channel over the long term. (3) Convex long profiles can develop under a range of ephemeral or perennial conditions, but where climate may not be the first-order control. All of these profile shapes exist within GLoPro

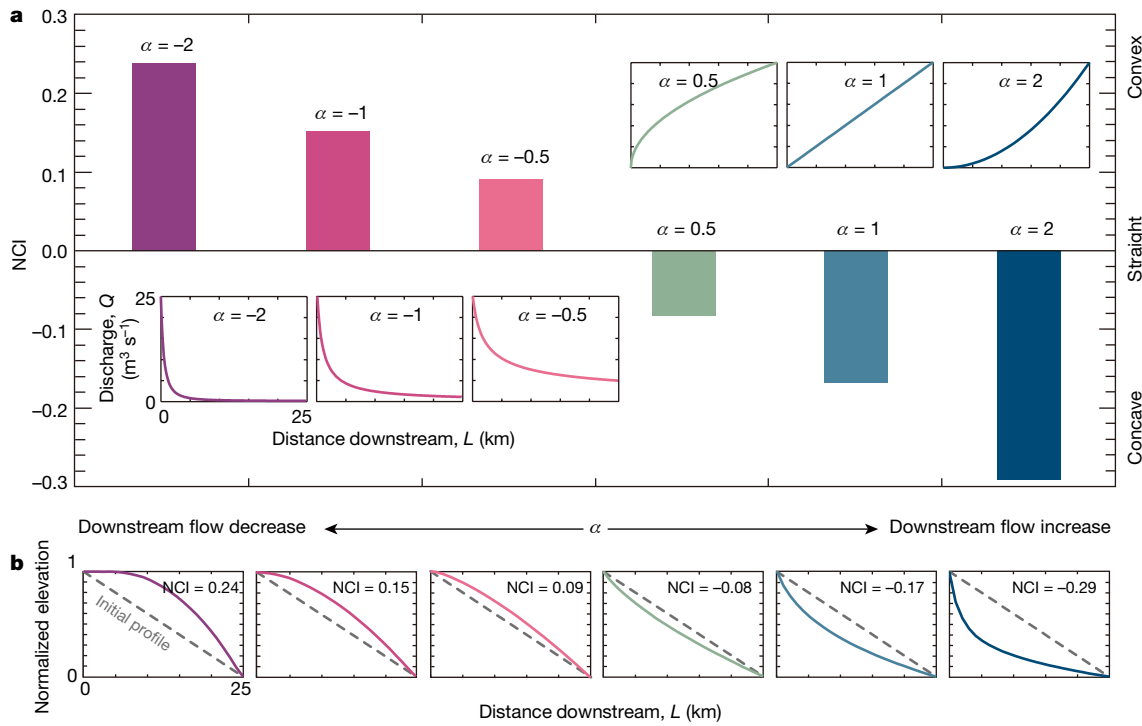


Fig. 3 | Modelling river long profiles with various downstream rates of flow change. a, NCI values for long profiles simulated with LONGPRO with a range of power-law exponents of the downstream rate of flow change (α). The inset panels show the corresponding downstream

distributions of discharge (Q) for various α values used in the LONGPRO modelling. b, Simulated river long profiles for the corresponding values of α , normalized by total river relief (the difference between maximum and minimum elevations of the long profile).

(Figs. 1, 2) with a preponderance of concave-up profiles in all climate zones (modelled large positive α), numerous straight profiles concentrated in arid regions (modelled small $|\alpha|$), and a smaller set of convex-up river profiles (modelled negative α) occurring in humid (strong orographic effects⁵) and arid regions (partial area contribution²³ and transmission losses²²). The effect of α in transport-limited rivers (and by extension, the effect of c in supply-limited rivers) overprints other plausible controls on profile concavity on the global scale (Extended Data Fig. 6).

Our global dataset, GLoPro, combined with simple numerical modelling and hydrological data analysis, has provided an explanation for how the hydrological expression of climate can produce systematic differences in long profile shapes based on aridity. From this global analysis of longitudinal profiles, we demonstrate that climatic signals are etched into river long profiles, irrespective of the variety of environmental conditions and other forcings across the globe (Methods). Despite overlaps in the NCI distributions, the overriding signal is one of aridity affecting channel flow and the cascade of drivers from climate to hydrology to erosion, corroborating previous studies^{8,10,31–33}. These findings highlight the importance of hydrological regimes, directly affected by climate, as a first-order control on the development of river topography, enhancing our understanding of drainage basin evolution in response to climate and climate change.

Online content

Any methods, additional references, Nature Research reporting summaries, source data, extended data, supplementary information, acknowledgements, peer review information; details of author contributions and competing interests; and statements of data and code availability are available at <https://doi.org/10.1038/s41586-019-1558-8>.

Received: 27 July 2018; Accepted: 3 July 2019;
Published online: 16 September 2019

- Tucker, G. E. & Slingerland, R. Drainage basin responses to climate change. *Wat. Resour. Res.* **33**, 2031–2047 (1997).
- Ferrier, K. L., Huppert, K. L. & Perron, J. T. Climatic control of bedrock river incision. *Nature* **496**, 206–209 (2013).
- Perron, J. T., Richardson, P. W., Ferrier, K. L. & Lapôtre, M. The root of branching river networks. *Nature* **492**, 100–103 (2012).
- Wolman, M. G. & Gerson, R. Relative scales of time and effectiveness of climate in watershed geomorphology. *Earth Surf. Processes* **3**, 189–208 (1978).
- Roe, G. H., Montgomery, D. R. & Hallet, B. Effects of orographic precipitation variations on the concavity of steady-state river profiles. *Geology* **30**, 143–146 (2002).
- Han, J., Gasparini, N. M., Johnson, J. P. & Murphy, B. P. Modeling the influence of rainfall gradients on discharge, bedrock erodibility, and river profile evolution, with application to the Big Island, Hawai'i. *J. Geophys. Res. Earth Surf.* **119**, 1418–1440 (2014).
- Zaprowski, B. J., Pazzaglia, F. J. & Evenson, E. B. Climatic influences on profile concavity and river incision. *J. Geophys. Res. Earth Surf.* **110**, <https://doi.org/10.1029/2004JF000138> (2005).
- Sólyom, P. B. & Tucker, G. E. Effect of limited storm duration on landscape evolution, drainage basin geometry, and hydrograph shapes. *J. Geophys. Res. Earth Surf.* **109**, <https://doi.org/10.1029/2003JF000032> (2004).
- Collins, D. & Bras, R. Climatic and ecological controls of equilibrium drainage density, relief, and channel concavity in dry lands. *Wat. Resour. Res.* **46**, <https://doi.org/10.1029/2009WR008615> (2010).
- Harel, M.-A., Mudd, S. & Attal, M. Global analysis of the stream power law parameters based on worldwide ^{10}Be denudation rates. *Geomorphology* **268**, 184–196 (2016).
- Hack, J. T. *Studies Of Longitudinal Stream Profiles In Virginia And Maryland*. Report 294B (US Government Printing Office, 1957).
- Phillips, J. D. & Lutz, J. D. Profile convexities in bedrock and alluvial streams. *Geomorphology* **102**, 554–566 (2008).
- Leopold, L. B. & Wolman, M. G. *Fluvial Processes in Geomorphology* (General Publishing, 1964).
- Snow, R. S. & Slingerland, R. L. Mathematical modeling of graded river profiles. *J. Geol.* **95**, 15–33 (1987).
- Vogel, J. Evidence of past climatic change in the Namib Desert. *Palaeogeogr. Palaeoclimatol. Palaeoecol.* **70**, 355–366 (1989).
- Singer, M. B. & Michaelides, K. How is topographic simplicity maintained in ephemeral dryland channels? *Geology* **42**, 1091–1094 (2014).
- Michaelides, K., Hollings, R., Singer, M. B., Nichols, M. H. & Nearing, M. A. Spatial and temporal analysis of hillslope-channel coupling and implications for the longitudinal profile in a dryland basin. *Earth Surf. Process. Landf.* **43**, 1608–1621 (2018).

18. Whipple, K. X. & Tucker, G. E. Dynamics of the stream-power river incision model: implications for height limits of mountain ranges, landscape response timescales, and research needs. *J. Geophys. Res. Solid Earth* **104**, 17661–17674 (1999).
19. Tucker, G. E. & Bras, R. L. Hillslope processes, drainage density, and landscape morphology. *Wat. Resour. Res.* **34**, 2751–2764 (1998).
20. Wickert, A. D. How should we estimate river discharge from drainage area? In *AGU Fall Meeting Abstract EP21D–2294* (AGU, 2018).
21. Lague, D., Hovius, N. & Davy, P. Discharge, discharge variability, and the bedrock channel profile. *J. Geophys. Res. Earth Surf.* **110**, <https://doi.org/10.1029/2004JF000259> (2005).
22. Knighton, A. & Nanson, G. Distinctiveness, diversity and uniqueness in arid zone river systems. In *Arid Zone Geomorphology: Process, Form and Change in Drylands 2nd edn*, 185–203 (John Wiley & Sons, 1997).
23. Yair, A., Sharon, D. & Lavee, H. An instrumented watershed for the study of partial area contribution of runoff in the arid zone. *Z. Geomorphol.* **29**, 71–82 (1978).
24. Jaeger, K. L., Sutfin, N. A., Tooth, S., Michaelides, K. & Singer, M. Geomorphology and sediment regimes of intermittent rivers and ephemeral streams. In *Intermittent Rivers and Ephemeral Streams* 21–49 (Elsevier, 2017).
25. Fan, Y., Li, H. & Miguelz-Macho, G. Global patterns of groundwater table depth. *Science* **339**, 940–943 (2013).
26. Farr, T. G. et al. The shuttle radar topography mission. *Rev. Geophys.* **45**, <https://doi.org/10.1029/2005RG000183> (2007).
27. Clubb, F. J., Mudd, S. M., Milodowski, D. T., Grieve, S. W. D., & Hurst, M. D. LSDChannelExtraction version v1.0, <https://doi.org/10.5281/zenodo.824198> (2017).
28. Peel, M. C., Finlayson, B. L. & McMahon, T. A. Updated world map of the Köppen-Geiger climate classification. *Hydroclim. Earth Syst. Sci. Discuss.* **4**, 439–473 (2007).
29. Trabucco, A. & Zomer, R. J. *Global Aridity and PET Database* <http://www.cgiar-csi.org/data/global-aridity-and-pet-database> (CGIAR Consortium for Spatial Information, 2009).
30. Slingerland, R., Harbaugh, J. W. & Furlong, K. *Simulation Clastic Sedimentary Basins: Physical Fundamentals and Computer Programs for Creating Dynamic Systems* (Prentice Hall, 1994).
31. Seybold, H., Rothman, D. H. & Kirchner, J. W. Climate's watermark in the geometry of stream networks. *Geophys. Res. Lett.* **44**, 2272–2280 (2017).
32. Bonnet, S. Shrinking and splitting of drainage basins in orogenic landscapes from the migration of the main drainage divide. *Nat. Geosci.* **2**, 766–771 (2009).
33. Molnar, P., Anderson, R. S., Kier, G. & Rose, J. Relationships among probability distributions of stream discharges in floods, climate, bed load transport, and river incision. *J. Geophys. Res. Earth Surf.* **111**, <https://doi.org/10.1029/2005JF000310> (2006).

Publisher's note: Springer Nature remains neutral with regard to jurisdictional claims in published maps and institutional affiliations.

© The Author(s), under exclusive licence to Springer Nature Limited 2019

METHODS

Köppen–Geiger and Aridity Index classifications. Our four main Köppen–Geiger climate zones²⁸ were compiled by aggregating the Af, Am and Aw sub-zones into the Tropical zone; the BWh, BWk, BSh and BSk sub-zones into the Arid zone; the Cs, Cw and Cf sub-zones into the Temperate zone; and the Ds, Dw and Df sub-zones into the Cold zone. We excluded Polar zones from the Köppen–Geiger dataset because of their tendency to be covered by permafrost or glaciers, making them subject to predominantly glacial processes rather than fluvial ones, and also to match the latitude constraints of the SRTM-DEM dataset²⁶. We acquired the spatial distribution of the Aridity Index along each river profile from the Global Aridity and PET Database²⁹, and then calculated the median Aridity Index value for each river.

One may wonder whether the prevailing climate in any basin may have shifted during or since profile development and how that might affect our results. In this study, we opted to use climate metrics that can currently be measured on a global basis, since they represent the best available information for analysis of a global river profile dataset. Having confirmation from two climatic indices (Köppen–Geiger and Aridity Index), which are computed in distinct ways, gives us confidence that we have captured real climate influences on long profile development. There will undoubtedly be examples where marked biome or climate shifts occurred during or since profile development within a region. However, given that we observed clear relationships between current climate classifications and NCI, we believe there is a strong case for contemporary climatic control on the profile. We suspect that any major climatic changes over or since the period of profile development would be captured as noise of the GLoPro dataset.

River long profile extraction. Using the Köppen–Geiger climate zones²⁸, the global SRTM-DEM²⁶ was broken into contiguous climate zone tiles, before any topographic processing was performed. This ensured that only rivers that were contained within a given climate zone would be extracted, and that any climatic signal contained within river long profile geometry would not be distorted by a river crossing climate zones. This means that the GLoPro dataset is limited to river basins that are typically $<2,500 \text{ km}^2$ in area and $<400 \text{ km}$ in length (Extended Data Fig. 4). In some cases, the contiguous climate zone tiles were still too large to be processed efficiently, and so these tiles were subdivided into smaller tiles using a quadtree algorithm. This processing resulted in 1,366 individual DEM tiles, each with an approximate spatial resolution of 30 m, which could be processed in parallel. To ensure the validity of measurements of river long profile geometry, and the ability to accurately compare measurements at a global scale, each DEM tile was projected into the appropriate Universal Transverse Mercator (UTM) coordinate system. Our method, applied to the entire SRTM dataset, optimizes the quality and internal consistency of the topographic information extracted into GLoPro, but it comes at the expense of precise geographical information owing to spatial variability in the projection of the dataset. This means that it may be challenging to match up GLoPro stream locations accurately to Geographic Information System (GIS) stream layers from other databases.

The topographic analysis of each of these tiles was performed using LSDTopoTools²⁷, an open source topographic analysis package designed to facilitate robust, reproducible analysis of DEM data. The first processing step was to correct each DEM tile hydrologically, to ensure that no artificial sinks were present. This was performed using an algorithm³⁴ that minimizes the topographic change required to ensure all DEM cells flow to the DEM base level. Following this, each cell in the DEM that exceeded a threshold drainage area, and that had no upslope cells (also exceeding the threshold), were identified as channel initiation points. The FastScape algorithm³⁵ was then applied to these initiation points to route flow efficiently downslope in the direction of steepest descent to generate a channel network for each tile. This steepest-descent method partitions flow from the DEM cell of interest to one of its eight neighbouring cells. From this generated network, the highest-order river (the longest channel) in each drainage basin or sub-basin that did not cross Köppen–Geiger sub-zone boundaries (Extended Data Fig. 1a) was extracted and incorporated into GLoPro.

Although more elaborate methods for channel extraction exist, it has been shown that these methods perform poorly on 30-m-resolution data³⁶, particularly in the upper reaches of catchments, where channel initiation points are known to be fine-scale features³⁷. The selection of a threshold drainage area is challenging, with considerable effort being expended on identifying techniques to constrain it³⁸. These challenges are magnified by the scale of this study, where the ideal threshold for a given area may be unsuitable for another. To resolve this issue, a deliberately conservative drainage area threshold of 25,000 pixels, equivalent to an area of 22.5 km^2 at the Equator, was applied. This value balances the need for computational efficiency with the requirement to confidently extract river elevation profiles³⁶.

We were concerned that our extraction method might yield false positives in areas where one would expect few channels (for example, dune fields such as the Sahara Desert). To check for this, we analysed the extracted channels from LSDTopoTools for part of The Grand Erg Oriental, Western Sahara. We found that

the results of the flow accumulation algorithm within LSDTopoTools showed flow between dunes along local topographic gradients and a coalescence of flow into a dominant channel that follows the regional topographic gradient (Extended Data Fig. 2). This is the channel that was extracted in our analysis for this area and that is included in GLoPro. It is plausible that under heavy rainfall, overland flow runoff would accumulate in this manner and would coalesce into a dominant channel that reworks dune sediment and leaves behind a topographic signature that is preserved. From arid lands literature on fluvial–aeolian feature interactions, we confirmed that it is common for interdune flow and coalescing flows (that is, ‘through-going’ fluvial channel networks) to cross entire aeolian dune fields and leave behind topographic signatures³⁹. Even after removing all major global dune fields from GLoPro, we found that our NCI results (showing systematically straighter long profiles with increasing aridity) are unaffected. It is worth mentioning that the fluvial channels included in GLoPro are based on a topographic definition—they represent a set of contiguous topographic positions in the landscape that would accumulate flow from upstream (should water be present) above a conservative threshold drainage area. A single point or a discontinuous series of points defined as a channel trace would not be extracted for inclusion in GLoPro. Instead, the extraction algorithm requires a consistent decline in elevation along the flow trace and an accumulation of upstream drainage area to define a channel. Accordingly, only longer channels in a basin or sub-basin would be included in our database. We view this definition as conservative, tending to rule out the inclusion of non-channel features (false positives) in our database.

For each DEM cell identified as a channel, topographic information was sampled to facilitate the creation of river long profiles, along with other relevant information about the river channel. This resulted in an average sampling frequency of 36 m along the length of each river, recording the elevation, flow length, drainage area, latitude and longitude of each cell. In addition to these topographic data, Aridity Index values were sampled at the centroid of every cell along the length of each river and the median Aridity Index value was calculated for the whole river. There are a small number of cases (40 rivers, or 0.01% of the dataset) where very few Aridity Index measurements (<10) were made along a river, owing to discrepancies between the spatial resolution of the Aridity Index data (around 900 m) and the SRTM dataset (around 30 m).

Given their source in SRTM data, the extracted profiles represent the water surface profile for perennial rivers and the bed topography profile for ephemeral rivers. The two profile types are comparable over the entire profile, as the water surface responds to the bed topography. Furthermore, NCI robustly captures the overall shape of the longitudinal profile, irrespective of the high-frequency variations associated with either riverbed or water surface profiles.

NCI. We define the endpoints of the longitudinal profile (L_0, E_0) and (L_n, E_n) where L is distance downstream, E is elevation, and where the subscripts 0 and n indicate the most upstream and downstream points, respectively. To calculate NCI, a straight line is fitted through the endpoints of the longitudinal profile described by the equation $Y_L = E_0 - \theta L$, where Y_L is the elevation on the line at each distance L , θ is the gradient of the line, and E_0 is the y intercept. Then, at each measured point along the profile, the vertical offset between the river profile and the fitted straight line is calculated as $E_L - Y_L$. We then calculate the median value of all offsets, normalized by the total topographic relief along the profile $(E_0 - E_n)$ to enable comparison across scales (Extended Data Fig. 1b). Therefore, NCI is defined as follows:

$$\text{NCI} = \text{median}[(E_L - Y_L)/(E_0 - E_n)] \quad (1)$$

Other concavity indices have been developed in the literature, such as the Stream Concavity Index (SCI)⁷, the Concavity Index (θ)⁴⁰, and the Chi (χ) transformation⁴¹. SCI, for example, calculates the area between channel elevation and the straight line connecting the endpoints of the channel, similarly to NCI. However, SCI is sensitive to local variations along the profile (for example, knickpoints) and requires smoothing. On the other hand, θ and χ are computed from the local channel gradient and upstream contributing drainage area and they are typically applied to multiple segments along the same river trace, rather than to summarize the concavity of an entire profile. Since our goal was to explore conditions where the relationship between area and channel discharge are weak for complete river profiles, we opted for a different metric. The advantages of NCI are that (1) it calculates all offsets of measured points at the native resolution of the measurements (DEM, field survey, model output); (2) it does not require any smoothing along the profile; (3) it does not require any assumptions about the relationship between slope and area or between area and river discharge; and (4) it can be used to quantify the concavity of a simulated profile (without considering basin area). The calculation of all vertical offsets along the profile enables the representation of local variations along the profile (for example, knickpoints), but the calculation of NCI is not sensitive to these variations (see Extended Data Fig. 3 for an example).

The river extraction methods and concavity calculation result in an internally consistent NCI dataset. The impact of the channel head location on NCI is minimal

because only the longest river of each basin or sub-basin was analysed (excluding smaller tributaries). We confirmed that NCI values for extracted rivers in GLoPro are not correlated with key river metrics, such as river length, gradient, relief or basin area (Extended Data Fig. 4). Therefore, we were confident in using NCI to compare rivers of different sizes and across climate zones.

The GLoPro database. *Database structure.* GLoPro is an SQLite database comprising two tables called ‘rivers’ and ‘profiles’. The ‘rivers’ table contains the following columns. (1) *uid*, which is a unique ID assigned by the database for each record. (2) *riverid*, which is the unique name given to each river record in GLoPro. It comprises the Köppen–Geiger climate zone that the river is within and a unique alphanumeric string. It is used to identify a given profile in the profile table. (3) *NCI*, which is the Normalized Concavity Index. (4) *koppen*, which is the Köppen–Geiger climate zone. (5) *geom*, which is a GeoJSON string containing the river geometry. It can be imported directly into any modern GIS package (for example, QGIS). For more information on the GeoJSON format see <http://geojson.org>.

The ‘profiles’ table contains the following columns. (1) *uid*, which is a unique ID assigned by the database for each record. (2) *riverid*, which is the unique name given to each river record in GLoPro. It comprises the Köppen–Geiger climate zone that the river is within and a unique alphanumeric string. It is used to identify the associated data for the river recorded in rivers. (3) *lat*, which is the latitude of the sampled point in decimal degrees. Spatial coordinates correspond to EPSG code 4326. (4) *long*, which is the longitude of the sampled point in decimal degrees. Spatial coordinates correspond to EPSG code 4326. (5) *length*, which is the cumulative flow length from the outlet of the river in metres. (6) *area*, which is the drainage area at a given point along a river, in square metres. (7) *AI*, which is the Aridity Index for a given point along the river. Aridity Index data are from <http://www.cgiar-csi.org/data/global-aridity-and-pet-database>.

Example queries. To select all of the data from the ‘rivers’ table, use `SELECT * FROM rivers`. To select all of the data from a given climate zone, use `SELECT * FROM rivers WHERE koppen like 'Af'`. To select rivers that have an NCI below a particular value, use `SELECT riverid FROM rivers WHERE NCI < -0.1`. To select the elevation and flow length of a given river, which can be used to plot a long profile, use `SELECT elevation, length FROM profiles WHERE riverid like 'Aw_75_river_72'`.

We note that owing to the size of the ‘profiles’ table, queries can take a few minutes to complete. To learn more about using SQL databases in a research context, we recommend the training materials provided by Software Carpentry (<http://swcarpentry.github.io/sql-novice-survey>).

KDE. In Fig. 2a–d, we present plots generated based on KDE. KDE is a non-parametric representation of the probability density function for the sample data. To show the distribution of NCI values of each climate zone, we used the built-in function `ksdensity` in MATLAB. Since the bandwidth of the kernel smoothing window affects the distribution shape, which leads to a smoother shape at higher bandwidth, we kept the bandwidth constant at an appropriately smoothed value of 0.02 for all climate zones (Fig. 2a–d). However, we also tested the estimations with various bandwidths for Köppen–Geiger classification, from 0.005 to 0.04. All results show that NCI distributions of the Arid zone skewed towards zero compared to three main humid zones, irrespective of the choice of bandwidth.

Two-sample Kolmogorov–Smirnov test. Statistical differences of the NCI distributions were analysed using the Kolmogorov–Smirnov test between distribution pairs across climate zones. The Kolmogorov–Smirnov test is a nonparametric test for checking whether two continuous, one-dimensional data samples, X_1 and X_2 , come from the same distribution. We used the built-in function `kstest2` in MATLAB to calculate the statistics and corresponding P values between Köppen–Geiger and Aridity Index categories (Extended Data Fig. 5). Since the number of sampled rivers is very large, the P values of all comparisons are lower than 2.1×10^{-20} . However, in Köppen–Geiger climate zones, comparisons between the Arid zone and all other zones yield P values lower than 4.27×10^{-190} (Extended Data Fig. 5a). Within the Aridity Index classes, smaller P values result when comparing categories that are further apart in terms of aridity (for example, the Hyper-Arid zone versus the Humid zone) (Extended Data Fig. 5b). These results support the conclusion that long profile shapes are distinct between arid and humid regions.

LONGPRO modelling. LONGPRO is a one-dimensional numerical model that simulates the dynamic evolution of the river long profile, and can be used to explore responses to varying water discharge, sediment supply, riverbed grain size, tectonic uplift and base level³⁰. LONGPRO includes gradually varied flow, sediment transport by Yang’s unit stream power equation⁴² and conservation of mass. We used LONGPRO to explore the relative controls on longitudinal profile development. Our goal was not to explore the parameter space of LONGPRO exhaustively, but rather to look at first-order effects of downstream discharge variation on the profile development for transport-limited conditions in a manner that is analogous to the supply-limited case generalized by stream power incision theory.

Given the large variance in drainage basin properties across the globe, we fixed several parameters in LONGPRO in order to isolate the effects of the climate expression within streamflow, and the corresponding impact on long profile evolution. We assumed no tectonic uplift and no base level change (but see below for a sensitivity analysis of these and other factors). We set river length to 25 km, a value similar to the median value of all extracted rivers (26.7 km). We set initial profile slope to 0.003, representing a linear decline from 75 m elevation at the upstream profile point (that is, E_0) to 0 m at the downstream point (E_n). Base level (the elevation of river water level above the riverbed at the most downstream point) was set at a constant value of 5 m. The maximum water discharge (Q_{\max}) was set as $25 \text{ m}^3 \text{ s}^{-1}$. Sediment-related parameters in LONGPRO include sediment supply at the upstream boundary (MFEED), sediment concentration of lateral inflow to the mainstem (SEDCON), the median grain size of bed material (DIMID), and Manning’s roughness coefficient (n). For these parameters, we set the following values as constants: MFEED to 10 kg s^{-1} , DIMID to 1 mm (uniform grain size along the profile), and n to 0.04. SEDCON was set to 0.00005 (the proportion of sediment concentration delivered by lateral tributary inputs), which follows the formula:

$$q_{s,L} = \text{SEDCON}(Q_L - Q_{L-1})(\Delta t) \quad (2)$$

where $q_{s,L}$ is the mass of lateral sediment supply at the distance downstream, L , which enters over timestep Δt . We note that for downstream decreasing discharge, we exchanged the positions of Q_L and Q_{L-1} in equation (2), in order not to get a negative $q_{s,L}$ value. The distance between calculated nodes was set as 1 km, and the timestep Δt was set to 24 h. The models were run for 500 years of effective discharge, by which time the rate of change to the profile became relatively small. In fact, the model tended to adjust to near-steady-state conditions very rapidly, rendering the model results insensitive to the initial profile, as per the model’s design³⁰. Since effective discharge tends to be expressed for much briefer periods (for example, bankfull discharge is often assumed to have a return period of about 1.5 years), the model simulation time actually represents a much longer period than 500 years of topographic adjustment.

We varied the downstream rate of change in streamflow, α , to explore the effects of climatically driven streamflow on long profile evolution in LONGPRO. To do this, we modified the LONGPRO code to enable the power-law exponent α to vary from positive to negative values:

$$Q_L = Q_n(L/L_n)^\alpha \quad (3)$$

where Q_L is the discharge at the distance downstream L , Q_n is the discharge of the most downstream point, and L_n is the river length. For downstream increasing discharge, Q_n equals Q_{\max} ($25 \text{ m}^3 \text{ s}^{-1}$). However, for downstream decreasing discharge, Q_{\max} occurs at the most upstream point (Q_0) and Q_n is calculated from equation (3) for the given α value. In this manner, we simulated variations in downstream discharge and their impact on long profile evolution. For each simulation, we generated a longitudinal profile for which we calculated the NCI. A range of simulated profiles from LONGPRO and associated NCI values for varying values of α are shown in Fig. 3.

Since other model parameters can also affect long profile concavities, we conducted sensitivity analyses to discharge (Q_{\max}), median grain size (DIMID), tectonic uplift and base level change. To model tectonic uplift in LONGPRO, we applied the maximum uplift rate at the most upstream point (0.1 mm yr^{-1} and 1 mm yr^{-1}), and the rate decreased linearly downstream to zero at the most downstream point. To model base level change, LONGPRO uses a simple sine function to represent base level variation. We set the amplitude and period of the sine curve to represent continuous base level decline (10 mm yr^{-1} and 50 mm yr^{-1}). The results of these various sensitivity analyses show that α is the dominant control of long profile concavity, overprinting other factors (Extended Data Fig. 6). Moreover, the other exogenous factors that are often assumed to control long profile evolution have a lesser effect than the expression of downstream hydrology.

Calculation of α values from real rivers. To develop a real-world understanding of α and its variation in different climate zones, we downloaded multidecadal mean daily streamflow data for rivers from the US Geological Survey’s National Water Information System (<https://waterdata.usgs.gov/nwis>). For each main Köppen–Geiger climate zone, we selected 5 rivers, spanning a range of river lengths, with at least three gauging stations along the same river (a total of 20 rivers), ensuring via Google Earth satellite imagery, that there are no obvious anthropogenic factors that could influence the downstream variation in discharge. The Köppen–Geiger classification was used as a mask for river selection by climate zones within the USA. The selected rivers needed to fulfill the following criteria: (1) at least three gauging stations on the same river for calculating α values; (2) no apparent influence of urban areas, irrigation or dams; and (3) no crossing between main Köppen–Geiger climate zones. We selected rivers distributed over different states with various lengths.

The median Aridity Index of each river was calculated so that we could compare values between Aridity Index climate classes (Extended Data Table 2). We calculated the median discharge for each gauge over its record, and then estimated a best-fit power law trendline between discharge and distance downstream for each river (Extended Data Fig. 7). Then we extracted α for each power-law fit from equation (3) (Extended Data Table 2).

The results show that rivers in Tropical, Temperate and Cold zones exhibit median α values between 1.24 and 1.75 (downstream increasing discharge), whereas the Arid zone displays α values in the range from negative (downstream decreasing discharge) to positive (downstream increasing discharge) with a median close to zero ($\alpha = 0.14$) (Extended Data Fig. 8a).

We also used these data (82 gauging stations in 20 rivers) to explore the relationship between discharge and basin area. The results clearly show strong differences between the Arid zone and the other Köppen–Geiger climate zones. The non-arid zones show a positive relationship between Q and A ($Q = 0.02A^{0.91}$, correlation factor $R^2 = 0.73$), whereas the Arid zone shows a very weak dependency on basin area ($Q = 0.04A^{0.10}$, $R^2 = 0.01$). One recent study²⁰ extracted flow records from a wide range of rivers in the USA across climate zones and analysed the relationship between discharge and drainage area. That analysis showed that the discharge-drainage area exponent c (in the equation $Q \propto A^c$) decreases both with lower mean annual precipitation and as flood recurrence interval increases, probably owing to the decreasing probability of storms capable of generating runoff over progressively larger basin areas. The exponent for arid channels is closest to zero for small floods and increases slightly for higher flood recurrence intervals. This is the opposite of the trends in exponents for humid river channels. This analysis supports our assumption about a weak discharge-drainage area relationship in drylands. In other words, basin shape is less influential on discharge in arid zones.

However, the analysis of α values was not exhaustive. It was based on a small sample of rivers where there was sufficient data to make calculations. In addition, α is based on the full distribution of downstream variations in discharge over decadal timescales. This distribution will not dramatically change α between flood events for perennial rivers in humid climates. By contrast, α in dryland ephemeral channels will fluctuate from flood to flood between positive and negative values depending on the size, location and duration of each storm and the runoff it generates. It will also be influenced by the ephemerality (for example, the length of time between flows) (Extended Data Fig. 8b). Nevertheless, these results show the relative differences in α values between groups of rivers in different climate categories. This supports our selection of the α values used in LONGPRO simulations.

Data availability

The datasets generated and analysed during the current study are available at <https://doi.org/10.17636/01058162>.

Code availability

The code for river long profile extraction (LSDTopoTools), including the code for calculating NCI, is available on GitHub (<https://github.com/sgrieve/concavity>). The code for the LONGPRO model is available on the Community Surface Dynamics Modelling System (<https://csdms.colorado.edu/wiki/Model:LONGPRO>). The repository that contains all of the code is at <https://doi.org/10.5281/zenodo.3257656>.

34. Wang, L. & Liu, H. An efficient method for identifying and filling surface depressions in digital elevation models for hydrologic analysis and modelling. *Int. J. Geogr. Inf. Sci.* **20**, 193–213 (2006).
35. Braun, J. & Willett, S. D. A very efficient O(n), implicit and parallel method to solve the stream power equation governing fluvial incision and landscape evolution. *Geomorphology* **180**, 170–179 (2013).
36. Grieve, S. W., Mudd, S. M., Milodowski, D. T., Clubb, F. J. & Furbish, D. J. How does grid-resolution modulate the topographic expression of geomorphic processes? *Earth Surf. Dyn.* **4**, 627–653 (2016).
37. Montgomery, D. R. & Dietrich, W. E. Where do channels begin? *Nature* **336**, 232–234 (1988).
38. Tarboton, D. G., Bras, R. L. & Rodriguez-Iturbe, I. On the extraction of channel networks from digital elevation data. *Hydrol. Processes* **5**, 81–100 (1991).
39. Al-Masrahy, M. A. & Mountney, N. P. A classification scheme for fluvial–aeolian system interaction in desert-margin settings. *Aeolian Res.* **17**, 67–88 (2015).
40. Flint, J. J. Stream gradient as a function of order, magnitude, and discharge. *Wat. Resour. Res.* **10**, 969–973 (1974).
41. Royden, L. H., Clark, M. K. & Whipple, K. X. Evolution of river elevation profiles by bedrock incision: analytical solutions for transient river profiles related to changing uplift and precipitation rates. *Eos* 81, Fall Meeting Suppl. Abstract T62F-09 (AGU, 2000).
42. Yang, C. T. Incipient motion and sediment transport. *J. Hydraul. Div.* **99**, 1679–1704 (1973).

Acknowledgements M.B.S. was supported in part by the NSF (grants BCS-1660490 and EAR-1700555). We acknowledge the use of the UCL Legion High Performance Computing Facility (Legion@UCL), and associated support services, in the completion of this work. We thank R. Slingerland for sharing the code and providing advice on the LONGPRO model. We thank J. Willenbring for comments on an early version of the manuscript.

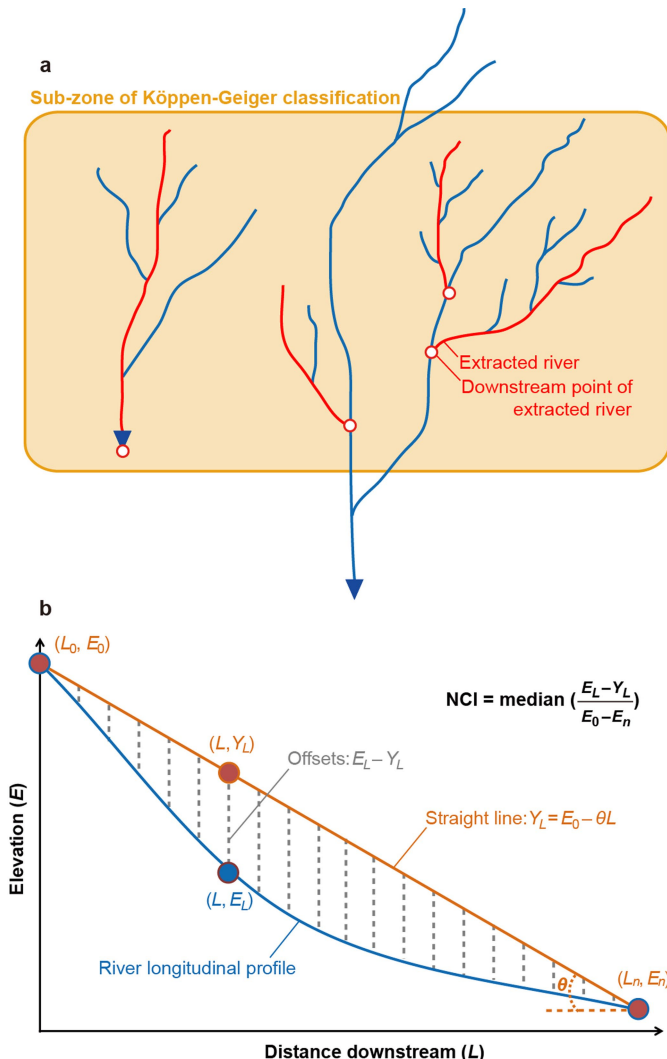
Author contributions K.M. and M.B.S. conceived the research and designed the study. S.W.D.G. extracted the river long profiles. S.-A.C. carried out the data analysis and model simulations. S.-A.C., K.M. and M.B.S. wrote the manuscript with contributions from S.W.D.G.

Competing interests The authors declare no competing interests.

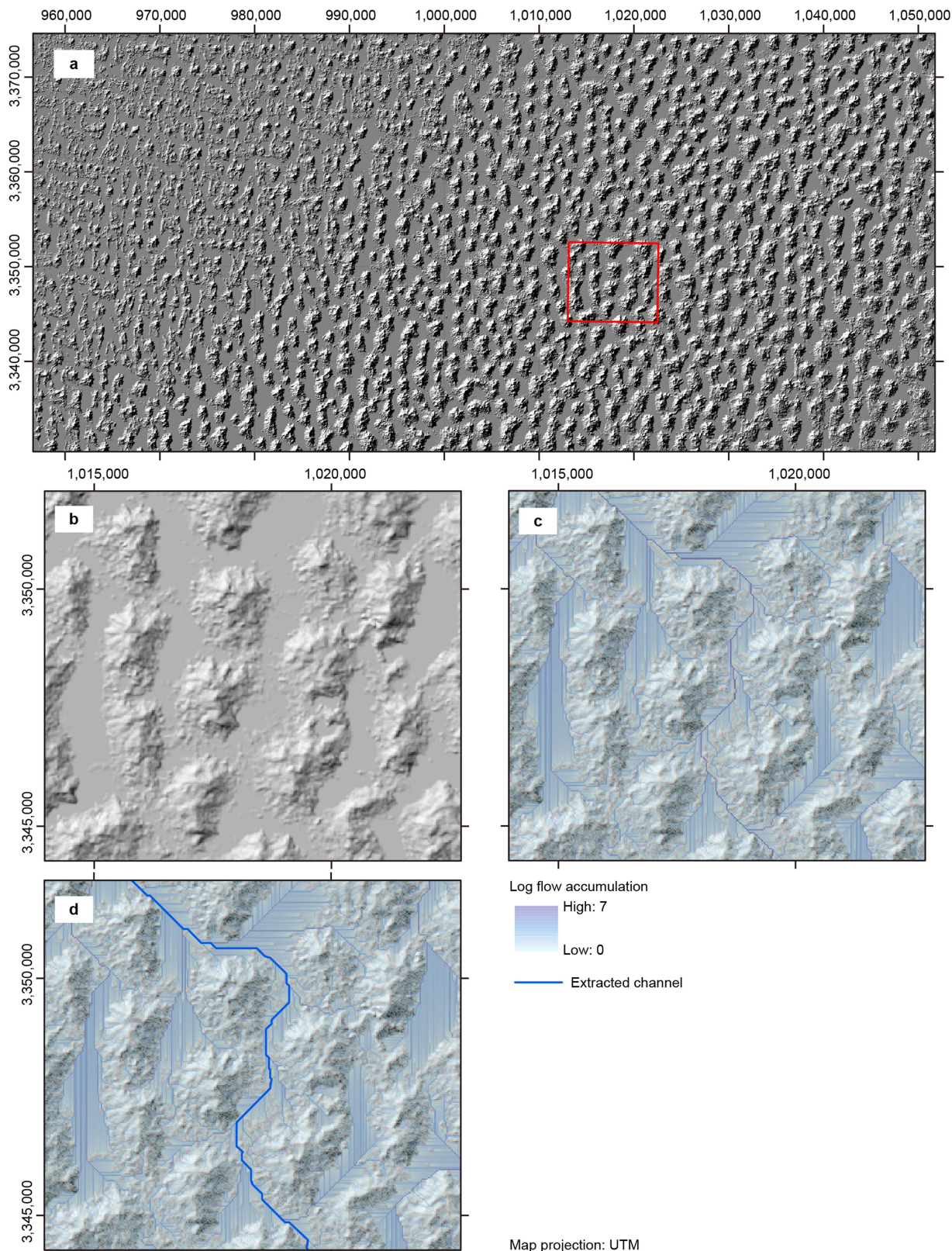
Additional information

Correspondence and requests for materials should be addressed to S.-A.C. or K.M.

Reprints and permissions information is available at <http://www.nature.com/reprints>.

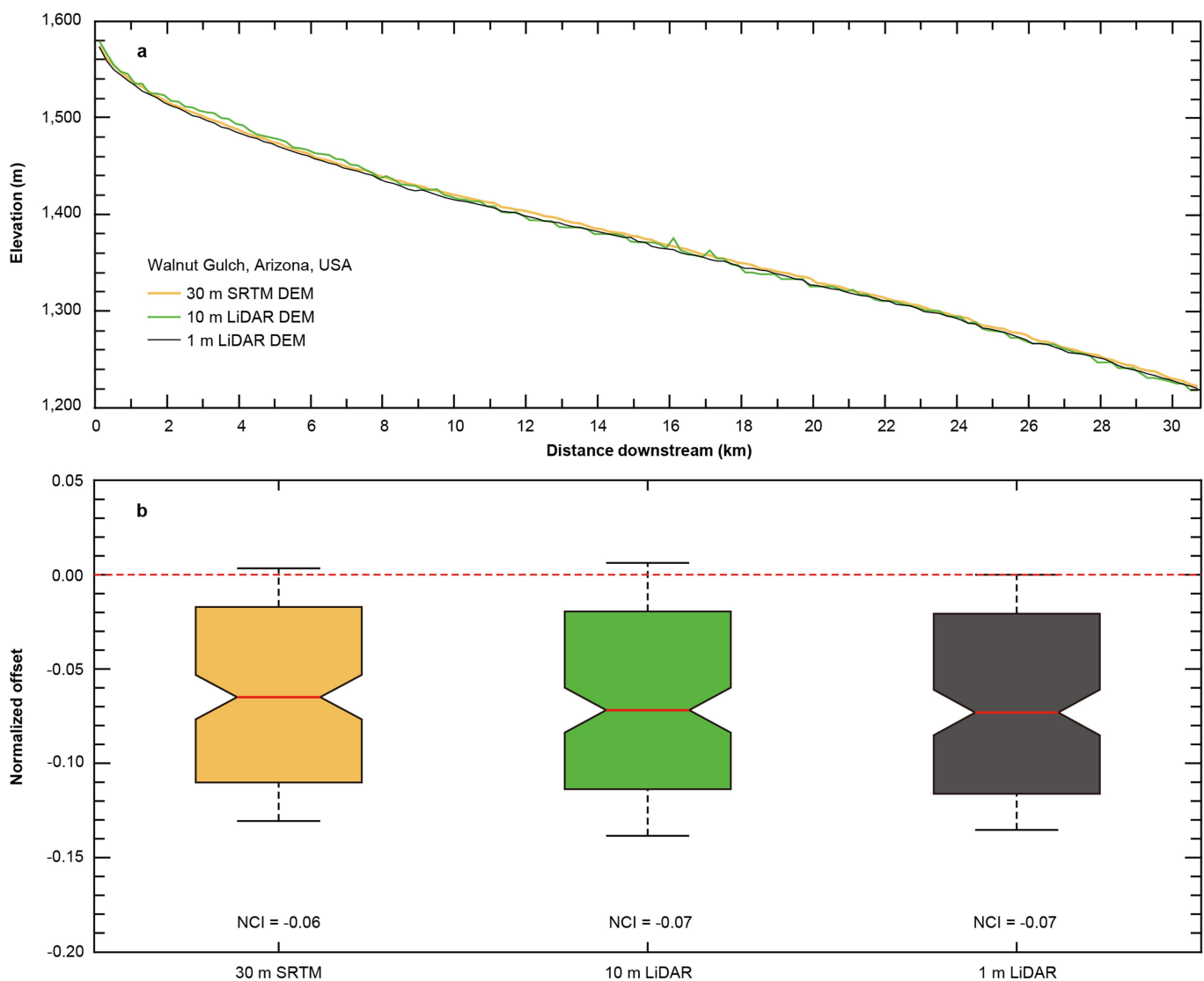


Extended Data Fig. 1 | Schematic of GLoPro river selection and NCI calculation. **a**, For each drainage basin, we selected the longest river that does not cross between Köppen–Geiger sub-zones. The schematic drainage system shows the rivers above the threshold drainage area in red (Methods), which were extracted into the GLoPro database. Extracted rivers could include the mainstem river of a whole basin (left) and/or its sub-basins (right). The longest river on the right (blue line) was not extracted, since it crosses Köppen–Geiger climate sub-zones. **b**, The blue line is a measured or modelled river long profile, and the orange line is the straight line fitted through the profile endpoints. The offset ($E_L - Y_L$) is the difference in elevations between the river long profile (E_L) and the straight line (Y_L) at each distance L . NCI is the median value of all offsets divided by topographic relief ($E_0 - E_n$). NCI is negative when the profile is concave, zero when the profile is straight, and positive if the profile is convex.



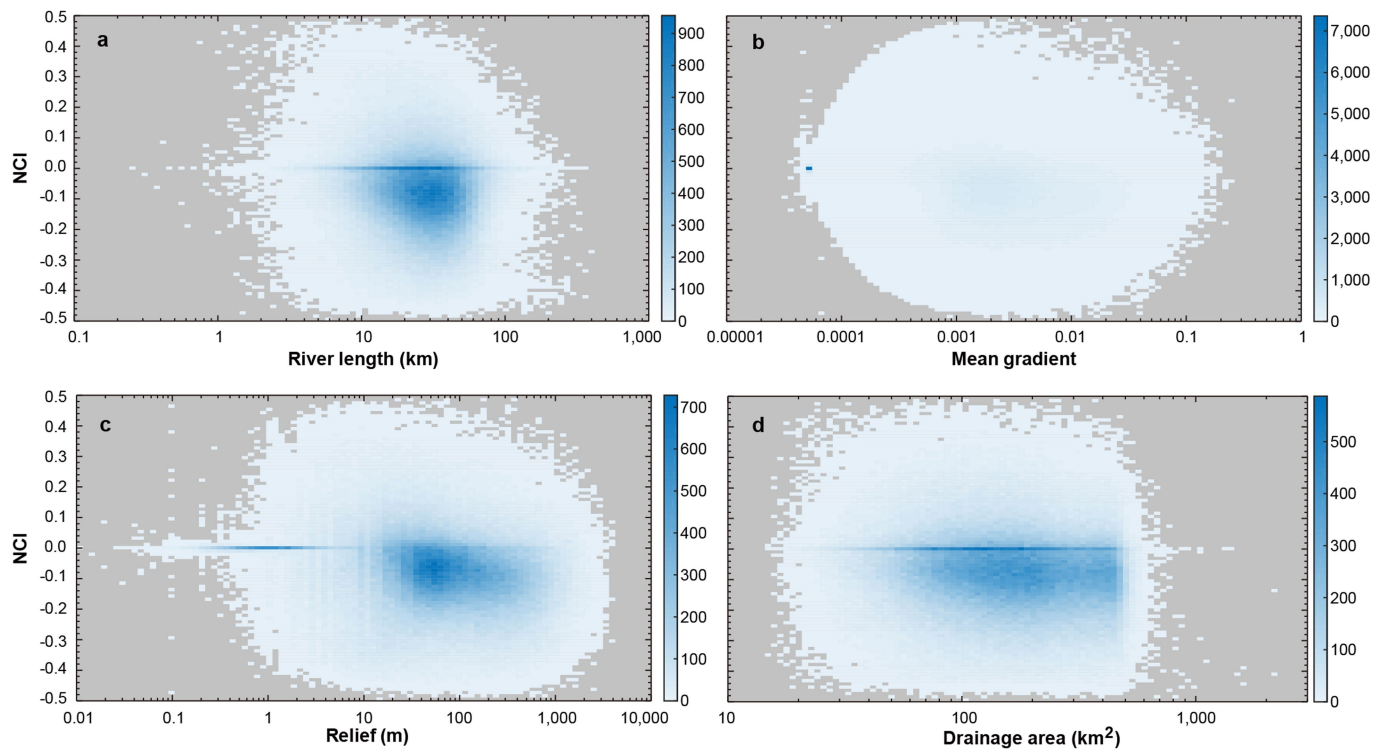
Extended Data Fig. 2 | Flow accumulation in The Grand Erg Oriental, Western Sahara. **a**, The wider context of the area. **b**, Close-up of the red rectangle in panel **a**. **c**, Flow accumulation traces derived

from LSDTopoTools. **d**, The extracted mainstem channel in the area representing the coalescence of flow traces into a dominant channel based on topography.



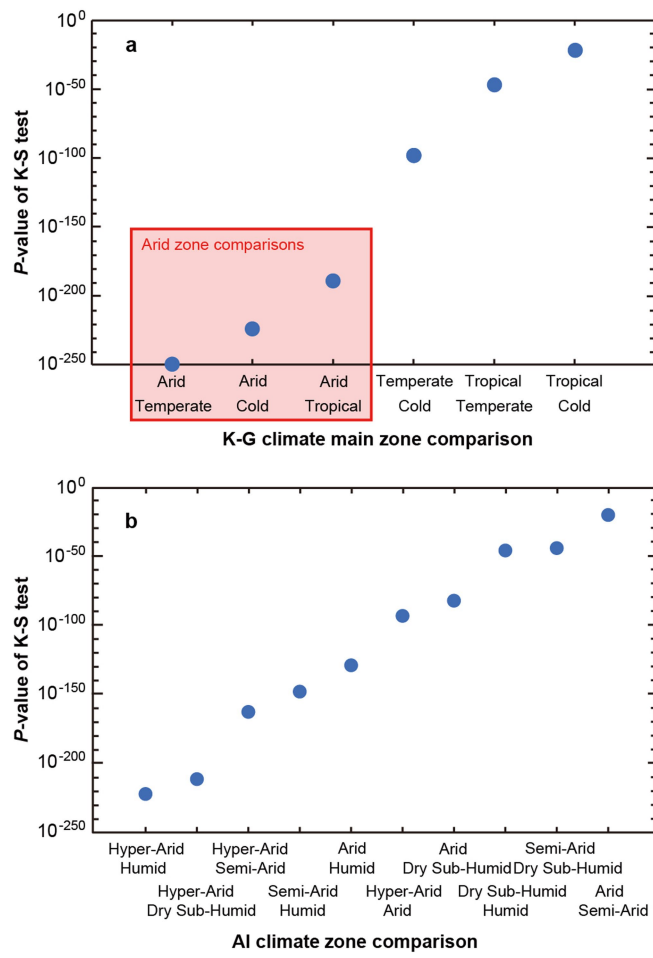
Extended Data Fig. 3 | River long profiles and NCI values for Walnut Gulch extracted from DEMs of varying resolutions. **a**, River long profiles extracted from SRTM and light detection and ranging (LiDAR) DEMs with different resolutions. **b**, Comparison of normalized offsets between river long profiles and the straight-line-fitted profile endpoints. Positive offsets indicate that the elevation of the river long profile is higher than the

straight line, whereas negative values mean the elevation of the long profile is lower than the straight line. The red dashed line indicates zero NCI (straight profiles). The red solid line in each boxplot represents the median offset value, which we define as the NCI value. These profiles show that DEM resolution has a minimal influence on NCI.

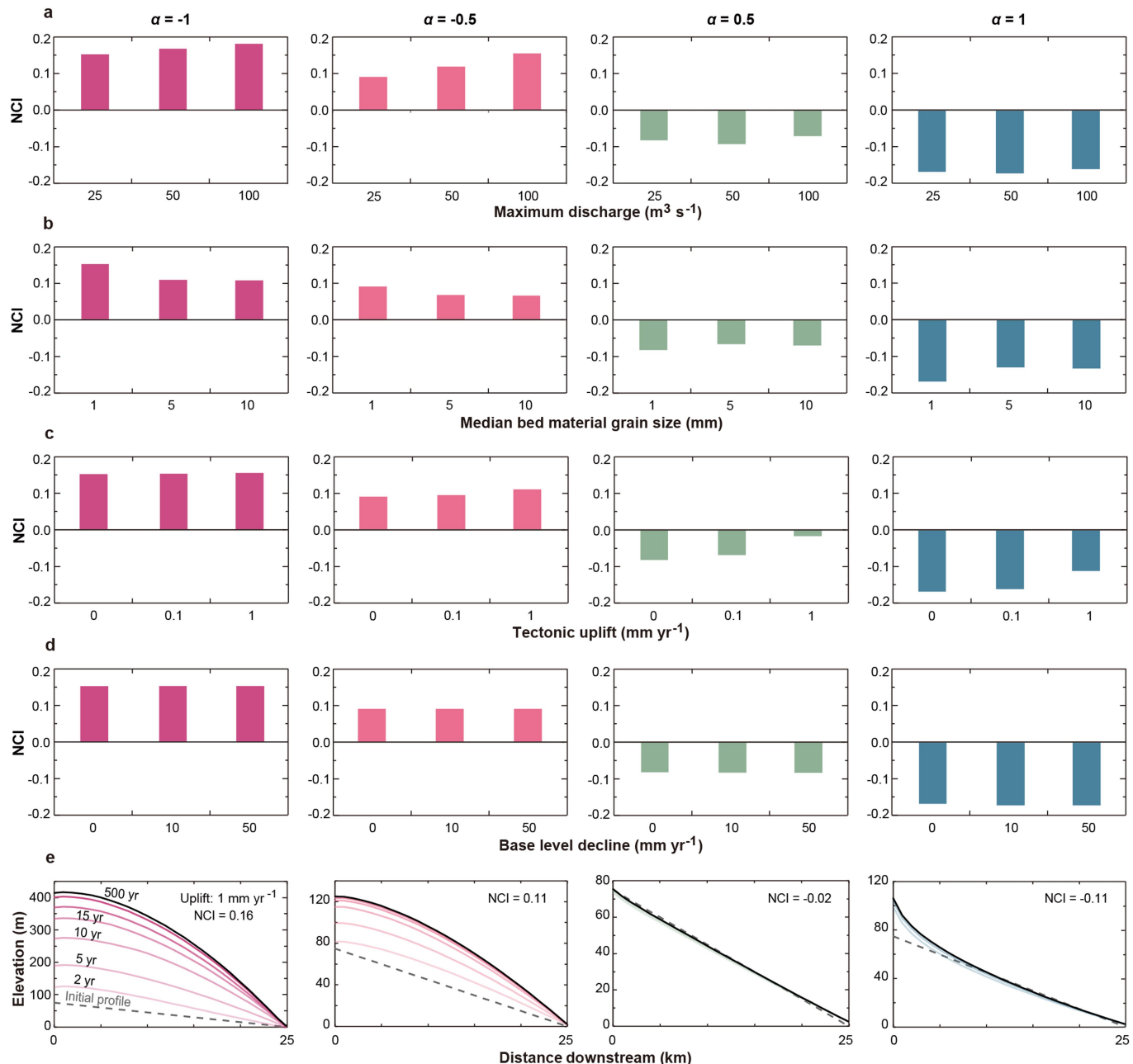


Extended Data Fig. 4 | Relationships between NCI and topographic metrics. **a**, Relationship between NCI and river length; **b**, Relationship between NCI and river gradient; **c**, Relationship between NCI and river relief; and **d**, Relationship between NCI and drainage area. The density of

points (number of rivers represented by each pixel) in the scatter plot is shown in the colour scales to the right of each panel. The results show no apparent relationship between NCI and any of these topographic metrics, suggesting that NCI is unbiased.

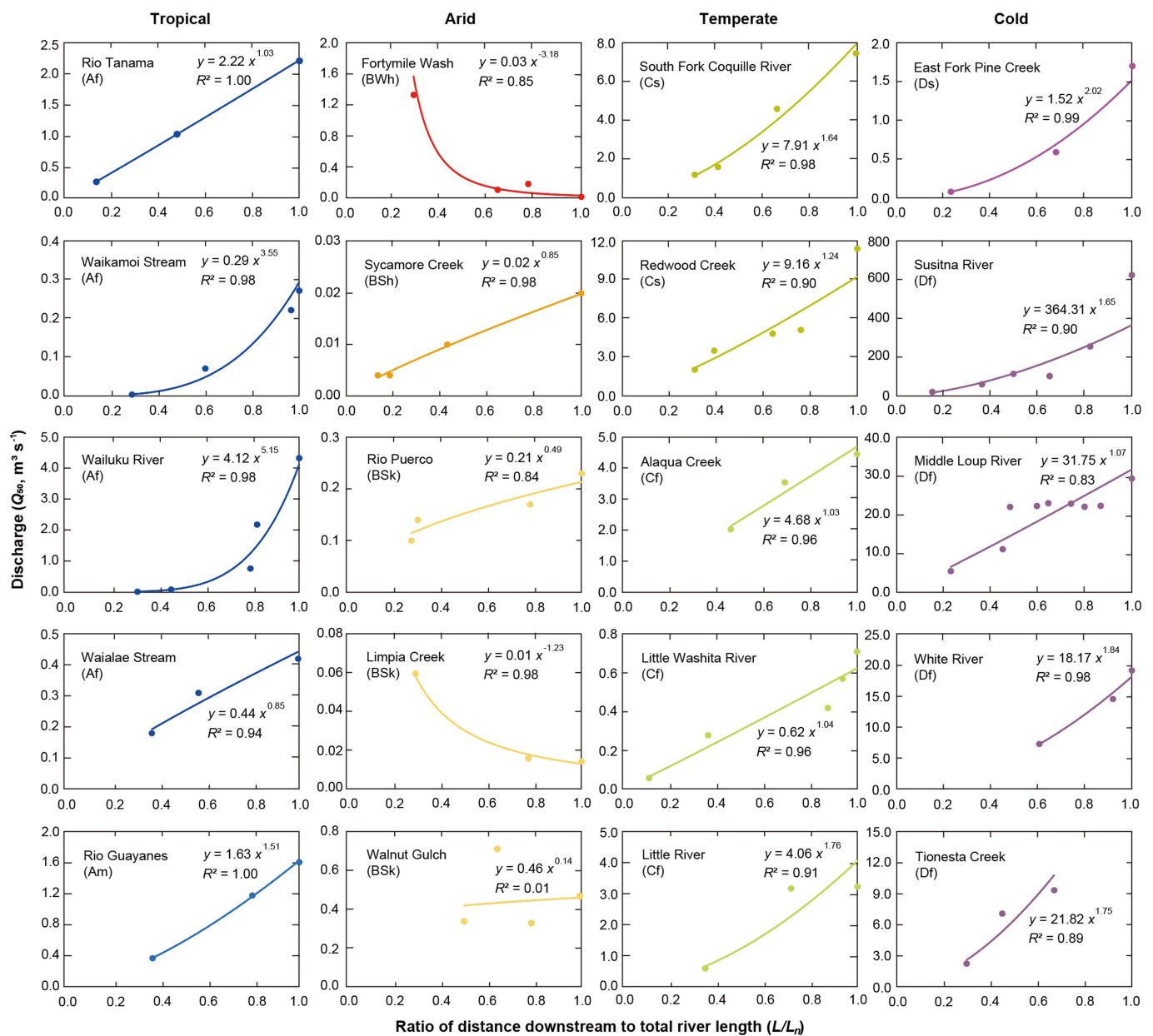


Extended Data Fig. 5 | Statistical differences of NCI distributions between climate zones. Graphical results of two-sample Kolmogorov–Smirnov (K–S) tests, which include the P values of NCI comparisons within the main Köppen–Geiger climate zones (a) and within the Aridity Index climate categories (b). The red box in panel a shows the comparisons involving the Arid zone, which all have smaller P values than other comparisons.



Extended Data Fig. 6 | Modelled NCI values for river long profiles simulated by LONGPRO generated with different forcings for various α values. **a**, NCI values for long profiles with various values of maximum discharge; **b**, NCI values for long profiles with various values of uniform median grain sizes of riverbed material; **c**, NCI values for long profiles with various values of tectonic uplift rates of the headwater; and **d**, NCI values for long profiles with various values of base level decline rates. All

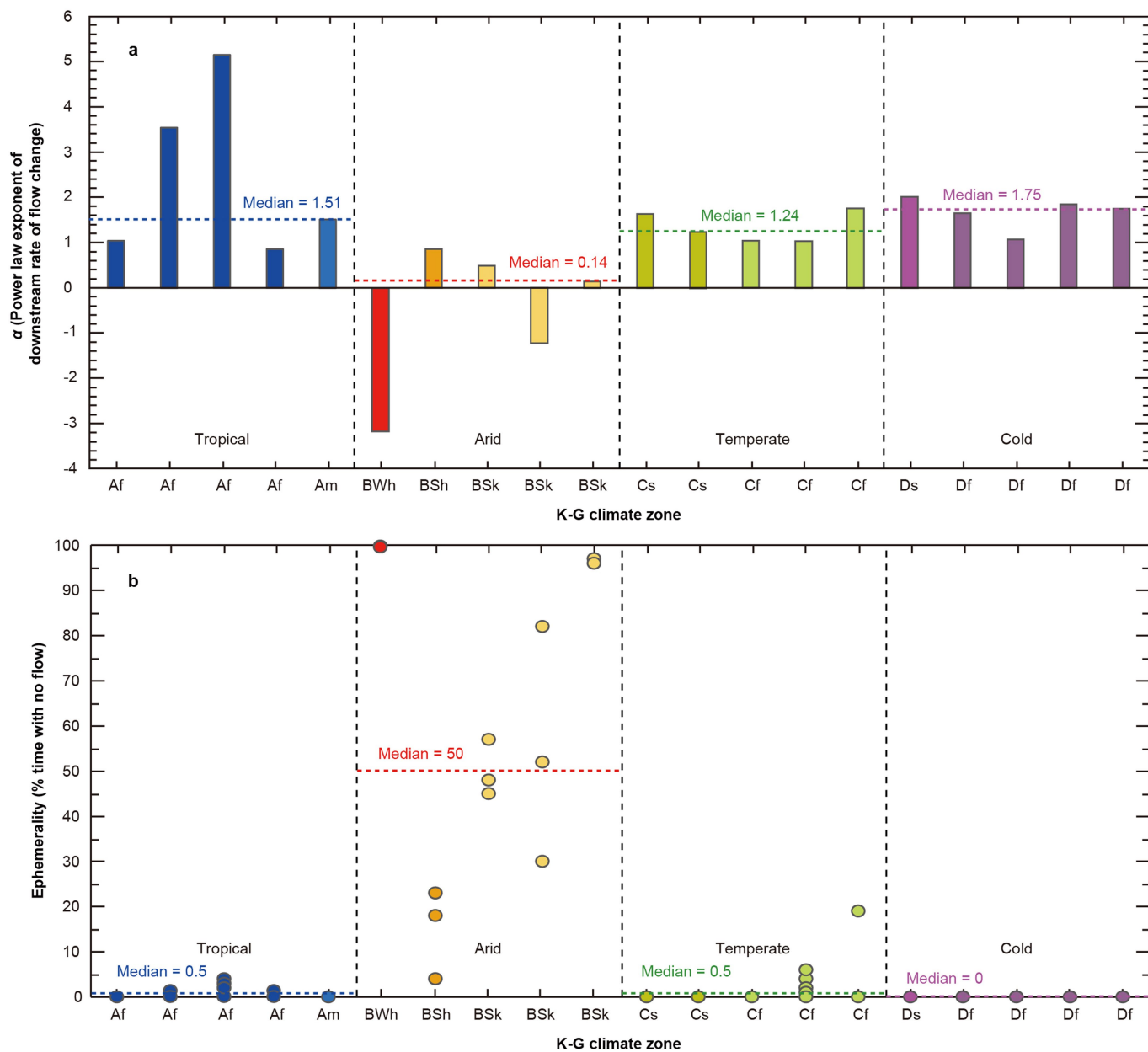
plots highlight the dominant effect of α on the river concavity. **e**, Long profile evolution with tectonic uplift (1 mm yr^{-1}), in which the profiles are shown for the initial profile (dashed line, the same for all simulations), 2 yr, 5 yr, 10 yr, 15 yr, 20 yr, 30 yr and 500 yr. The final simulated profile for each is indicated as a dark black line. The NCI values of final profiles for each value of α are also shown. Profiles evolve rapidly to near-steady-state conditions for all simulations.



Extended Data Fig. 7 | Calculation of α values from discharge data.

Power-law fits between median daily discharge (Q_{50}) and L/L_n (see equation (3) in the Methods) for each discharge gauging station are

shown for the selected rivers within the four main Köppen–Geiger climate zones in the USA (Extended Data Table 2). The colours and codes in brackets below each river name correspond to the Köppen–Geiger climate classification (Fig. 2).



Extended Data Fig. 8 | Comparison of α and ephemerality for selected rivers between the main Köppen–Geiger climate zones in the USA.
a, α values for each selected river; **b**, Corresponding values of ephemerality. The order of rivers is consistent with the data in Extended

Data Table 2. The colours correspond to the Köppen–Geiger climate classification (Fig. 2). Dotted lines indicate the median value for each main climate zone, showing that the Arid zone has a lower α and higher ephemerality compared to the others.

Extended Data Table 1 | Summary data on the number of rivers and summary statistics of NCI by Köppen–Geiger (K-G) and Aridity Index climate classifications

K-G climate sub-zone	Af	Am	Aw	BWh	BWk	BSh	BSk	Cs	Cw	Cf	Ds	Dw	Df	All														
Number of rivers	13,319	10,020	35,950	50,760	17,697	18,775	26,132	6,983	16,654	25,002	3,476	20,213	88,521	333,502														
K-G climate main zone																												
Number of rivers	Tropical			Arid			Temperate			Cold																		
Median of NCI																												
K-G climate main zone																												
Median of NCI	-0.083			-0.073			-0.081			-0.058																		
IQR of NCI																												
K-G climate sub-zone																												
IQR of NCI	0.188			0.176			0.141			0.130																		
K-G climate main zone																												
IQR of NCI	0.159			0.135			0.157			0.157																		
AI climate zone	Hyper-Arid			Arid			Semi-Arid			Dry Sub-Humid			Humid		All													
Number of rivers	21,070			56,571			63,925			33,499			156,759		331,824													
Median of NCI	-0.050			-0.068			-0.073			-0.084			-0.082		-0.075													
IQR of NCI	0.131			0.141			0.130			0.138			0.163		0.150													

Extended Data Table 2 | Data on α and ephemerality (percentage of time with no flow, ‘Ephe.’) for twenty rivers spanning the four main Köppen–Geiger climate zones within the USA

K-G zone	AI zone (AI value)	River name	State	Stations	Drainage area (km ²)	River length (km)	Q _n (m ³ s ⁻¹)	Ephe. (%)	α
Af	Humid (1.39)	Rio Tanama	Puerto Rico	50027850 50028000 50028400	57.50	39.93	2.22	0	1.03
Af	Humid (2.45)	Waikamoi Stream	Hawaii	16552800 16554000 16555000 16556000	10.31	11.62	0.29	0-1	3.55
Af	Humid (2.50)	Wailuku River	Hawaii	16701750 16701800 16703000 16704000 16713000	635.79	37.89	4.12	0-4	5.15
Af	Humid (2.49)	Waialae Stream	Hawaii	16019000 16020000 16021000	21.37	18.51	0.44	0-1	0.85
Am	Humid (1.15)	Rio Guayanes	Puerto Rico	50082800 50083500 50085100	68.89	21.17	1.63	0	1.51
BWh	Arid (0.13)	Fortymile Wash	Nevada	10251242 10251250 10251255 10251258	818.44	74.59	0.029	99.6-99.8	-3.18
BSh	Semi-Arid (0.33)	Sycamore Creek	Arizona	09510070 09510080 09510150 09510200	424.76	50.12	0.02	4-23	0.85
BSk	Arid (0.18)	Rio Puerco	New Mexico	08333500 08334000 08352500 08353000	16,109.73	369.01	0.21	45-57	0.49
BSk	Semi-Arid (0.27)	Limpia Creek	Texas	08431700 08431800 08432000	784.77	66.67	0.013	30-82	-1.23
BSk	Semi-Arid (0.22)	Walnut Gulch	Arizona	FLO001 FL002 FL006 FL009	149.33	30.80	0.46	96-97	0.14
Cs	Humid (1.69)	South Fork Coquille River	Oregon	14324600 14324700 14324900 14325000	437.71	55.35	7.91	0	1.64
Cs	Humid (1.39)	Redwood Creek	California	11481500 11482000 11482120 11482200 11482500	717.43	95.85	9.16	0	1.24
Cf	Humid (1.11)	Alaqua Creek	Florida	02366996 02367000 02367006	216.78	29.09	4.68	0	1.03
Cf	Dry Sub-Humid (0.59)	Little Washita River	Oklahoma	07327442 07327447 07327490 07327500 07327550	600.88	56.44	0.62	0-6	1.04
Cf	Humid (0.85)	Little River	Georgia	02317797 02318000 02318380	2,009.83	111.19	4.06	0-19	1.76
Ds	Humid (1.04)	East Fork Pine Creek	Idaho	12413360 12413370 12413445	189.59	13.61	1.52	0	2.02
Df	Humid (1.00)	Susitna River	Alaska	15291000 15291500 15291700 15292000 15292780 15294350	50,142.17	463.34	364.31	0	1.65
Df	Dry Sub-Humid (0.51)	Middle Loup River	Nebraska	06775000 06775500 06777000 06777500 06778000 06779000 06779500 06780000 06785000	8,106.66	365.24	31.75	0	1.07
Df	Humid (1.17)	White River	Vermont	01142000 01143500 01144000	1,787.09	82.45	18.17	0	1.84
Df	Humid (1.12)	Tionesta Creek	Pennsylvania	03017000 03017500 03018000 03019000	1,214.70	75.17	21.82	0	1.75